



# 1 **Lambda-PFLOTRAN 1.0: Workflow for Incorporating Organic** 2 **Matter Chemistry Informed by Ultra High Resolution Mass** 3 **Spectrometry into Biogeochemical Modeling**

4  
5 Katherine A. Muller<sup>1</sup>, Peishi Jiang<sup>1</sup>, Glenn Hammond<sup>1</sup>, Tasneem Ahmadullah<sup>1</sup>, Hyun-Seob Song<sup>2</sup>, Ravi Kukkadapu<sup>1</sup>,  
6 Nicholas Ward<sup>3</sup>, Madison Bowe<sup>3</sup>, Rosalie K. Chu<sup>1</sup>, Qian Zhao<sup>1</sup>, Vanessa A. Garayburu-Caruso<sup>1</sup>, Alan Roebuck<sup>3</sup>,  
7 Xingyuan Chen<sup>1</sup>

8 <sup>1</sup> Pacific Northwest National Laboratory, Richland, WA 99352, USA

9 <sup>2</sup> Department of Biological Systems Engineering, University of Nebraska—Lincoln, Lincoln, Nebraska, USA

10 <sup>3</sup> Pacific Northwest National Laboratory, Sequim WA 98382, USA

11 *Correspondence to:* Katherine Muller ([katherine.muller@pnnl.gov](mailto:katherine.muller@pnnl.gov))

12 For submission to Geoscientific Model Development

13 **Abstract.** Organic matter (OM) composition plays a central role in microbial respiration of dissolved organic matter  
14 and subsequent biogeochemical reactions. Here, a direct connection of organic carbon chemistry and thermodynamics  
15 to reactive transport simulators has been achieved through the newly developed Lambda-PFLOTRAN workflow tool  
16 that succinctly incorporates carbon chemistry data generated from Fourier transform ion cyclotron resonance mass  
17 spectrometry (FTICR-MS) into reaction networks to simulate organic matter degradation and the resulting  
18 biogeochemistry. Lambda-PFLOTRAN is a python-based workflow, executed through a Jupyter Notebook interface,  
19 that digests raw FTICR-MS data, develops a representative reaction network based on substrate-explicit  
20 thermodynamic modeling (also termed lambda modeling due to its key thermodynamic parameter  $\lambda$  used therein), and  
21 completes a biogeochemical simulation with the open source, reactive flow and transport code PFLOTRAN. The  
22 workflow consists of the following five steps: configuration, thermodynamic (lambda) analysis, sensitivity analysis,  
23 parameter estimation, and simulation output and visualization. Two test cases are provided to demonstrate the  
24 functionality of the Lambda-PFLOTRAN workflow. The first test case uses laboratory incubation data of temporal  
25 oxygen depletion to fit lambda parameters (i.e., maximum utilization rate and microbial carrying capacity). A slightly  
26 more complex second test case fits multiple lambda formulation and soil organic matter release parameters to temporal  
27 greenhouse gas generation measured during a soil incubation. Overall, the Lambda-PFLOTRAN workflow facilitates  
28 upscaling by using molecular-scale characterization to inform biogeochemical processes occurring at larger scales.  
29



## 30 **1 Introduction**

31 Microbial respiration of dissolved organic carbon (DOC) is a main driver of environmental biogeochemical processes.  
32 Mechanistic biogeochemical models often rely on lumping organic matter into a few distinct carbon pools (e.g.,  
33 dissolved, sorbed, mineral associated or refractory, labile, etc.) (e.g., Faticchi, et al., 2019, Robertson et al., 2019, Wang  
34 et al., 2013) but do not fully consider the properties of the organic matter (OM) compounds individually. Pooled  
35 carbon approaches have benefits, such as assigning variable levels of bioavailability, however, this approach does not  
36 capture the complex temporal dynamics of respiration driven by OM composition, as aerobic respiration rates have  
37 been linked to organic carbon concentration, thermodynamics of the OM (Stegen et al., 2018, Garayburu-Caruso et  
38 al., 2020), as well as the diversity of OM compounds present (Lehmann et al. 2020, Stegen et al., 2022). Such findings  
39 highlight the importance of incorporating individual OM chemistry into biogeochemical modeling to capture, and  
40 ultimately predict, system behavior more accurately.

41 There are many advanced instrumentation techniques capable of detecting and identifying individual OM formulae  
42 that comprise a bulk OM sample (e.g., GC-MS, HPLC-MS, Fourier transform ion cyclotron resonance mass  
43 spectrometry [FTICR-MS], etc.). For instance, FTICR-MS is a powerful, high-resolution, method that identifies  
44 molecular formulae for individual organic compounds. In any given environmental sample, FTICR-MS (or other ultra  
45 high-resolution methods) will typically resolve thousands of discrete OM molecular formulae, each with a unique  
46 mass and elemental composition (Cooper et al., 2020, Bahureksa et al., 2021). Unfortunately, untargeted analytical  
47 techniques like FTICR-MS are only able to determine if a compound is present and cannot quantify the total  
48 concentration associated with each organic matter molecule. Still, such techniques do provide immense amounts of  
49 characterization data encompassing a deeper analytical window than measuring a small number of individual  
50 biomarkers quantitatively (e.g., Ward et al., 2013). However, the ability to utilize such high-resolution molecular data  
51 in reactive transport modeling frameworks has remained a challenge and is typically not considered.

52 Substrate-explicit thermodynamic modeling (SXTM) provides an avenue for incorporating individual OM reactivity  
53 based on thermodynamics (Song et al., 2020) into reactive transport models. The SXTM procedure takes the individual  
54 chemical formula derived from FTICR-MS (or another high-resolution technique) and uses its thermodynamic  
55 properties to generate an oxidation reaction for each molecular formula present in a sample. The corresponding  
56 reaction stoichiometry is then determined by considering catabolic, anabolic, and metabolic reactions and balancing  
57 energy for the overall metabolic reaction, allowing for the development of an aerobic respiration expression for each  
58 OM formula.

59 Still, the sheer number of compounds identified in each sample proves difficult for model integration. Typically,  
60 reactive transport simulators consider only a small number of primary species in their reaction networks, and most  
61 could not support modeling each of the thousands of organic matter molecules individually. Here, the developed  
62 Lambda-PFLOTRAN workflow addresses this challenge through grouping, or binning, similar compounds based on  
63 their thermodynamic properties, allowing for the number of species considered within the reaction network to be  
64 reduced, and thus decreasing the required computational resources.

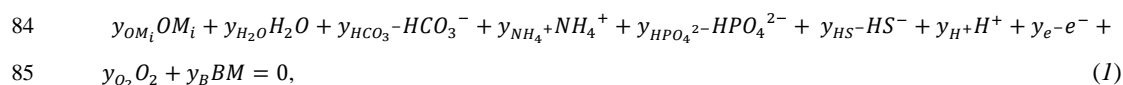


65 Lambda-PFLOTRAN is a python-based workflow that digests raw FTICR-MS data, develops a representative reaction  
66 network based on substrate-explicit thermodynamic modeling (Song et al., 2020), and completes a biogeochemical  
67 simulation with the open source, parallel reactive flow and transport code, PFLOTRAN (Hammond et al., 2014).  
68 PFLOTRAN is developed under an open source, GNU LGPL license. The term ‘lambda’ is used here because  $\lambda$  is a  
69 key parameter in the SXTM, which quantifies thermodynamic favorability of aerobic respiration of OM. The  
70 connection between the unique reaction network developed for each FTICR-MS sample hinges on the use of  
71 PFLOTRAN’s reaction sandbox capability (Hammond, 2022). The reaction sandbox gives the ability to define  
72 additional custom, kinetic reactions beyond standard formulations (e.g., mineral precipitation-dissolution, Michaelis-  
73 Menten, etc.). The Lambda-PFLOTRAN workflow enables upscaling by using molecular-scale information to inform  
74 larger scale biogeochemical processes occurring throughout a watershed which can be simulated with PFLOTRAN.  
75 Herein we describe the Lambda-PFLOTRAN workflow process including the governing expressions, workflow steps,  
76 data requirements, as well as the associated assumptions and limitations. Two illustrative test cases are also included  
77 to demonstrate the use of the workflow to utilize, parametrize, and model real datasets.

## 78 2 Methods

### 79 2.1 Conceptual Model

80 Respiration modeling herein is based on thermodynamic theory by Desmond-Le Quemener and Bouchez (2014) which  
81 was updated for multiple OM formulas by Song et al. (2020). The generalized form of OM molecule is assumed to  
82 take the form of  $C_aH_bN_cO_dP_eS^z_f$ . Each molecular formula then undergoes respiration (i.e., reaction with oxygen) based  
83 on the following general reaction expression:



86 This generalized expression is used to describe the oxidation of any OM molecule,  $i$ , and has been normalized to one  
87 mole of biomass (BM) produced. BM is assumed to have a formula of  $CH_{1.8}O_{0.5}N_{0.2}$  (Stephanopoulos et al.,  
88 1998; Kleerebezem and Van Loosdrecht, 2010).  $OM_i$  represents the OM molecules as informed by FTICR-MS. Each  
89  $y$  represents the reaction stoichiometry for that reactant ( $y < 0$ ) or product ( $y > 0$ ). While this expression is specific for  
90 cases where oxygen is the electron acceptor, such an expression could be updated for alternative electron acceptors.

91 Substrate-explicit thermodynamic modeling expressions developed from Song et al. (2020) were implemented in a  
92 reaction sandbox within PFLOTRAN. The expressions were implemented in a general manner allowing for flexibility  
93 in handling variations in FTICR-MS data and several user adjustable analysis configurations.

94 The microbial growth kinetics are described by Eq. (2):



$$95 \quad \mu_i^{kin} = \mu^{max} \exp\left(-\frac{\alpha|y_{OC,i}|}{1000V_h[OC_i]}\right) \exp\left(-\frac{\alpha|y_{O_2,i}|}{1000V_h[O_2]}\right), \quad (2)$$

96 where  $\mu_i^{kin}$  is the unregulated uptake rate of reaction for  $OM_i$  [ $hr^{-1}$ ],  $\mu^{max}$  is the maximal microbial growth rate [ $hr^{-1}$ ],  $y_{OM,i}$  is the stoichiometry for  $OM_i$  [ $mol-OM \cdot mol-biomass^{-1}$ ],  $V_h$  is microbial harvest volume [ $m^3$ ]. Given the  
 97  
 98 physical interpretation of  $V_h$  as the microbial harvest volume, it is assumed here that the value of  $V_h$  is the same for  
 99 both  $OM_i$  and  $O_2$ ,  $[OM_i]$  is the organic matter concentration of  $OM_i$  [ $mol-OM \cdot L^{-1}$ ],  $y_{O_2,i}$  is the stoichiometry for  $O_2$   
 100 for respiration of  $OM_i$  [ $mol-O_2 \cdot mol-biomass^{-1}$ ],  $[O_2]$  is oxygen concentration [ $mol-O_2 \cdot L^{-1}$ ],  $\alpha$  is a microbial unit  
 101 conversion [ $mol-biomass$ ] and is the conversion of  $m^3$  to L.

102 Further, using a cybernetic modeling approach (after Song et al., 2018), all the unregulated uptake rates ( $\mu_i^{kin}$ ) are  
 103 normalized by the sum of unregulated uptake rates across all reactions,  $i$  following Eq. (3):

$$104 \quad u_i = \frac{\mu_i^{kin}}{\sum_{i=1}^n \mu_i^{kin}} \quad (3)$$

105 where  $u_i$  is the fraction of the unregulated rate [-]. The final regulated rate,  $r_i$  [ $hr^{-1}$ ] for each reaction is then computed  
 106 following Eq. (4):

$$107 \quad r_i = u_i \mu_i^{kin}, \quad (4)$$

108 For implementation within PFLOTRAN, the use of inhibition terms was required to prevent negative concentrations  
 109 once a reactant is nearly depleted. For a reaction to proceed, all reactant species must be present above a minimum  
 110 concentration even if the molecules do not explicitly control the respiration rate (i.e., species other than  $OM$  and  $O_2$ ,  
 111 Eq. (2). If a reactant concentration falls below a threshold concentration, the respiration rate is inhibited. Reactant  
 112 inhibition is computed by Eq. 5 (Kinzelbach et al., 1991) for reactant species  $j$ :

$$113 \quad I_j = 0.5 + \frac{\arctan((C_j - C_{thj}) \cdot f)}{\pi}, \quad (5)$$

114 where  $C_{th,j}$  is the threshold concentration [M],  $f$  is the threshold scaling factor [-]. The default  $C_{th,j}$  is  $10^{-20}$  M.

115 The reaction rates are also inhibited by the microbial carrying capacity of the system,  $I_{cc}$ , as follows in Eq. (6):

$$116 \quad I_{CC} = 1 - \frac{[BM]}{CC} \quad (6)$$

117 where  $[BM]$  is the biomass concentration [ $mol-BM \cdot L^{-1}$ ],  $CC$  is the biomass carrying capacity [ $mol-BM \cdot L^{-1}$ ].  $I_{cc}$  has a  
 118 non-negativity constraint, so if  $[BM] > CC$ , then  $I_{cc} = 0$ .

119 These inhibition factors are applied to the overall rate expression as shown in Eq. (7).

$$120 \quad r_{i,inhibited} = r_i I_{CC} \prod I_j \quad \forall y_{i,j} < 0, \quad (7)$$

121 The overall individual species rates,  $d[C_j]/dt$ , [ $mol-species \cdot L^{-1} \cdot hr^{-1}$ ] are then computed as follows with Eq. (8):



122 
$$\frac{dc_j}{dt} = (\sum_{i=1}^n \gamma_{i,j} r_{i, inhibited}) [BM], \quad (8)$$

123 where  $j$  is the species index. The total number of species includes 7 general species (i.e.,  $\text{HCO}_3^-$ ,  $\text{NH}_4^+$ ,  $\text{HPO}_4^-$ ,  $\text{HS}$ ,  
124  $\text{H}^+$ ,  $\text{O}_2$ ,  $\text{BM}$  (i.e., Eq (1)) and the OM species considered (i.e., typically 10).  $i$  is the reaction index,  $n$  is total number  
125 of reactions as based on the total number of OM species (typically, with this workflow  $n=10$ ).  $\gamma_{i,j}$  is the coefficient  
126 for species  $j$  in reaction  $i$ .

127  
128 The expression for biomass is also modified to account for biomass decay (note all biomass stoichiometries are 1 by  
129 definition):

130 
$$\frac{dBM}{dt} = (\sum_{i=1}^n \gamma_{i,j} r_{i, inhibited}) [BM] - k_{deg} [BM], \quad (9)$$

131 where  $k_{deg}$  is the biomass decay rate [ $\text{hr}^{-1}$ ].

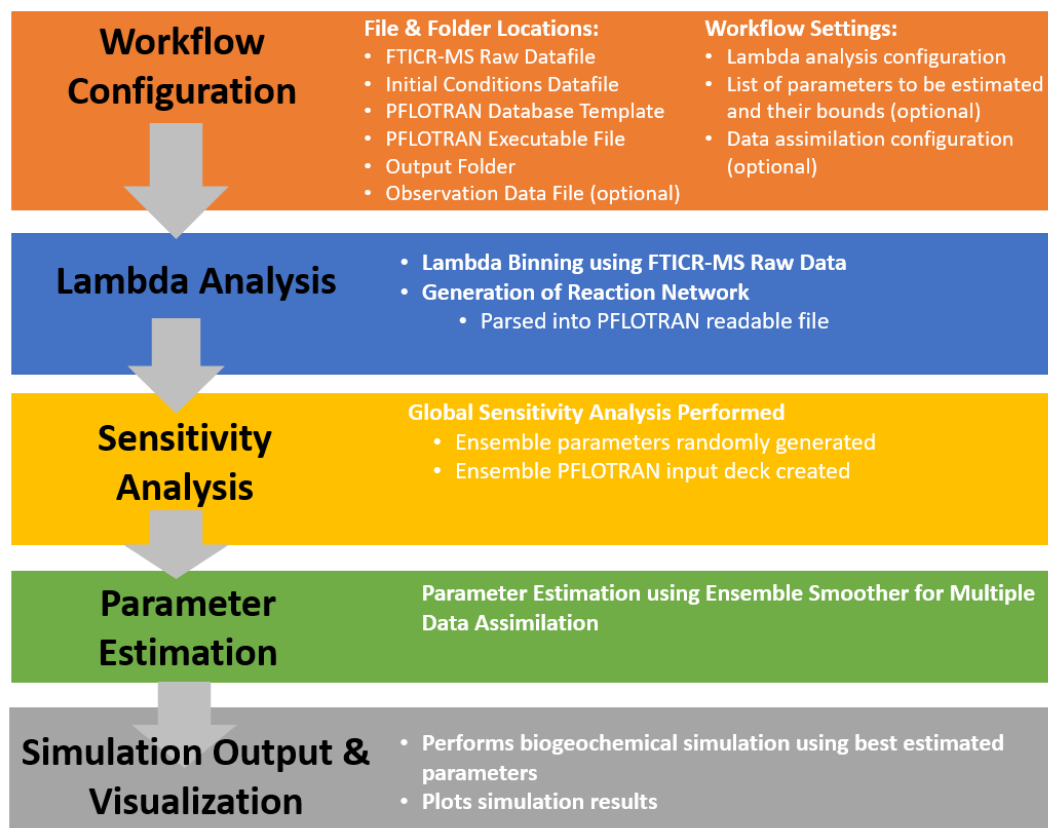
132

### 133 **2.2 Lambda Analysis and Binning**

134 To reduce the number of organic compounds considered in the simulation, OM molecules are grouped, or binned,  
135 based on their  $\lambda$  value computed by Eq. (10):

136 
$$\lambda = \frac{\Delta G_{r, anabolic} + \Delta G_{r, dissipation}}{(-\Delta G_{r, catabolic})}, \quad (10)$$

137 where  $\Delta G$  are the Gibbs energies for the anabolic and catabolic reactions and the associated dissipation energy,  
138 respectively. The value of  $\lambda$  is indicative of how many times the catabolic reaction needs to be completed to provide  
139 the energy required to synthesis one mole of biomass. Lower  $\lambda$  values suggest higher thermodynamic favorability of  
140 OM respiration. Using the chemical formula determined for each OM molecule, the energy balance equations are  
141 solved providing the overall reaction stoichiometry Eq. (1) and the  $\lambda$  is calculated. Using the  $\lambda$  value for each molecule,  
142 the cumulative probability distribution for the sample is produced (Figure 2).

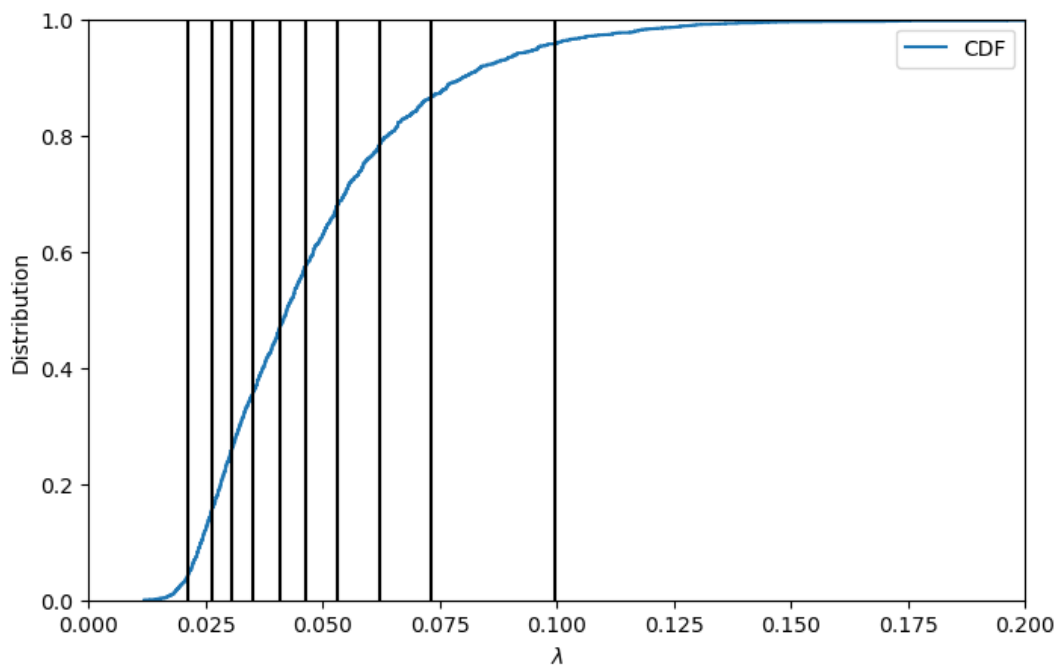


143

144 **Figure 1:** Flow Chart of the Lambda-PFLOTRAN Workflow.

145

146 It is this conversion from individual compounds to a distribution that is critical for reducing the entire sample down  
147 to a representative set of expressions. The  $\lambda$  bins are then formed by splitting the cumulative probability distribution  
148 into equally weighted sections as which to define the overall sample by. The illustrative example shown in Fig. 2  
149 demonstrates the sample distribution being divided into 10 sections (i.e., in this case each section contains 10% of the  
150 overall sample distribution).



151

152 **Figure 2:** Lambda binning to convert raw FTICR-MS into a representative reaction network using the cumulative probability  
 153 distribution function (CDF) for Test Case 1a. Vertical lines display the average  $\lambda$  value for each of the 10 bins (left to right,  $\lambda$  bin  
 154 1 to 10).

155

156 Each section is used to determine a representative organic matter formula and the associated reaction and  
 157 stoichiometry of that  $\lambda$  bin. The group of representative reactions (one per bin) is called the reaction network. A  
 158 demonstrative reaction network defined by  $\lambda$  analysis and binning is shown in Table 1.

159

160 **Table 1:** Reaction Network Developed from Lambda Theory for Test Case 1a

Bin Number	Representative Organic Matter Species Formula	$\lambda$	$y_{OC}$	$y_{HCO_3^-}$	$y_{NH_4^+}$	$y_{HPO_4^{2-}}$	$y_{HS^-}$	$y_{H^+}$	$y_{O_2}$
1	$C_{31}H_{44}N_{0.33}O_{4.8}P_{0.6}S_{0.3}$	0.021	-0.05	0.64	-0.17	-0.18	0.03	0.02	-1.07
2	$C_{26}H_{39}N_{0.20}O_{7.0}P_{0.6}S_{0.1}$	0.026	-0.07	0.68	-0.10	-0.19	0.04	0.01	-1.06
3	$C_{22}H_{36}N_{0.24}O_{7.5}P_{0.5}S_{0.1}$	0.031	-0.08	0.69	-0.02	-0.18	0.04	0.01	-1.06
4	$C_{20}H_{32}N_{0.28}O_{7.3}P_{0.4}S_{0.1}$	0.035	-0.08	0.72	-0.08	-0.18	0.04	0.01	-1.05
5	$C_{19}H_{29}N_{0.48}O_{7.9}P_{0.3}S_{0.2}$	0.041	-0.09	0.79	-0.17	-0.16	0.03	0.02	-1.04
6	$C_{18}H_{26}N_{0.68}O_{8.1}P_{0.2}S_{0.2}$	0.046	-0.10	0.85	-0.27	-0.13	0.02	0.02	-1.03
7	$C_{17}H_{24}N_{0.69}O_{8.1}P_{0.2}S_{0.2}$	0.053	-0.11	0.90	-0.32	-0.12	0.02	0.02	-1.02
8	$C_{15}H_{20}N_{0.67}O_{7.6}P_{0.2}S_{0.2}$	0.062	-0.13	0.94	-0.42	-0.11	0.02	0.03	-1.00



9	$C_{13}H_{19}N_{1.13}O_{87.4}P_{0.1}S_{0.2}$	0.073	-0.15	1.01	-0.48	-0.03	0.01	0.03	-1.00
10	$C_{10}H_{15}N_{1.56}O_{6.5}P_{0.1}S_{0.2}$	0.100	-0.21	1.17	-0.75	0.12	0.01	0.04	-0.97

161

162 Currently, the representative OM molecule that defines each bin is computed as the average chemical formula of all  
163 the molecules present in that  $\lambda$  section. The disadvantage of this approach is that unrealistic compounds are defined  
164 as representative molecules instead of realistic molecules. The issue with selecting a single, but real compound, from  
165 within each  $\lambda$  section resides in chemical complexity and variation - for instance some molecules may contain low  
166 levels of phosphorous or sulfur and others may not contain either element in the chemical formula. Thus, requiring  
167 the representative chemical formula to be a real compound present in the sample would create basis which would  
168 propagate through the reaction network and into the resulting biogeochemical simulation results.

### 169 2.3 Lambda-PFLOTTRAN Workflow

170 The Lambda-PFLOTTRAN workflow digests raw FTICR-MS data, calculates the  $\lambda$  distribution for the sample,  
171 generates the  $\lambda$  bins and corresponding reaction network, and completes a biogeochemical simulation using  
172 PFLOTTRAN. Further, we incorporated sensitivity analysis and ensemble data assimilation to enable an in-depth  
173 exploration of the impact of reaction parameters on respiration as well as a straightforward parameter estimation  
174 method to fit model parameters to experimental data.

175 The workflow is implemented through a user-friendly Jupyter notebook interface (Kluyver et al., 2016) where a user  
176 can configure the simulation parameters by adjusting initial concentrations,  $\lambda$  binning configuration, parameter values  
177 and/or ranges, and data assimilation options. Based on the user's data file and the associated parameters, scripts within  
178 the Jupyter notebook write the corresponding PFLOTTRAN input files, including OM molecules and aqueous  
179 chemistry. The PFLOTTRAN simulations are completed locally through a Docker container making this capability  
180 much more user-friendly and accessible. The progress of the data assimilation tool used for parameter fitting is  
181 illustrated within the Jupyter notebook. The resulting best fit final biogeochemical simulation is output visually with  
182 plots and as a text file (when applicable).

183 The Lambda-PFLOTTRAN workflow steps are shown in Figure 1 and described in detail in the following subsections:

#### 184 2.3.1 Step 1 – Workflow configuration

185 The first step is to set up the workflow configuration for a Lambda-PFLTORAN application. This includes specifying  
186 the file and folder locations of the following information: 1) FTICR-MS raw data file (.csv), 2) initial species  
187 concentrations file (.csv) that includes starting molar concentrations for  $HCO_3^-$ ,  $NH_4^+$ ,  $HPO_4^{2-}$ ,  $HS^-$ ,  $H^+$ ,  $O_2$  (aq), BM  
188 and total organic carbon (TOC), 3) PFLOTTRAN database template file, 4) PFLOTTRAN executable file, 5) workflow  
189 output folder, and if completing parameter estimation, (6) the data observation file (.csv), if applicable.

190 The user is also asked to configure workflow settings related to: (1) the lambda analysis configuration, including  
191 number of  $\lambda$  bins and method to define the  $\lambda$  bins (i.e., cumulative vs uniform); (2) the respiration modeling parameter





192 setup, including the list of the parameters to be estimated and their associated upper and lower bounds and (3) the data  
193 assimilation configuration (see below).

### 194 2.3.2 Step 2 – Organic Matter Chemistry using Lambda Analysis

195 With only an input of FTICR-MS data, the workflow first performs the lambda analysis (Section 2.2) to group OM  
196 molecules into various  $\lambda$  bins based on each compound's thermodynamics (Figure 2) and produce the corresponding  
197 reaction network for respiration (Table 1). The default number of  $\lambda$  bins is 10, although this can be adjusted in the  
198 workflow configuration by the user, if desired. The generated reaction network is then automatically parsed by the  
199 workflow into a text file that can be read by PFLOTRAN.

### 200 2.3.3 Step 3 – Sensitivity Analysis using Mutual Information

201 This step performs the global sensitivity analysis on the parameters to be estimated. Ensemble parameters are first  
202 generated by randomly sampling from their predefined ranges in the configuration step and saved into an HDF5 file.  
203 Then, the workflow generates a PFLOTRAN input deck to conduct ensemble simulations using the ensemble  
204 parameters. The generated ensemble model states enables a global sensitivity analysis using mutual information  
205 (Cover and Thomas, 2006; Jiang et al, 2022) as follows:

$$206 \quad I(X; Y) = H(Y) - H(Y|X) = \sum_{x=x} \sum_{y=y} p(x, y) \log \left( \frac{p(x, y)}{p(x)p(y)} \right), \quad (11)$$

207 where  $x$  and  $y$  are the specific values of  $X$  and  $Y$ , respectively;  $H(Y)$  is the Shannon's entropy of  $Y$ ;  $H(Y|X)$  is the  
208 conditional entropy of  $Y$  given  $X$ ;  $p$  is the probability density function. Higher  $I$  indicate stronger sensitivity between  
209  $X$  and  $Y$ . Besides sensitivity analysis, the ensemble parameter/states also serve as the prior information for parameter  
210 estimation at the next step.

### 211 2.3.4 Step 4 – Parameter Estimation using Ensemble Smoother for Multiple Data Assimilation

212 The workflow adopts Ensemble Smoother for Multiple Data Assimilation (Emerick and Reynolds, 2013; Jiang et al,  
213 2021), abbreviated as ESMDA, for data assimilation in this step. Rooted in ensemble Kalman filter, ESMDA is an  
214 iterative data assimilation approach that assimilates the observations on the entire time period for multiple times to  
215 reduce the uncertainty of the estimated or posterior parameters. During each iteration of ESMDA, the model  
216 parameters are updated based on the following equation:

$$217 \quad m_{k,l}^u = m_{k,l}^f + C_{MD,l}^f (C_{DD,l}^f + \alpha_l C_D)^{-1} \left( d_{obs} + \sqrt{\alpha_l} C_D^{\frac{1}{2}} z_k - d_{k,l}^f \right), \quad k = 1, \dots, N_e \text{ and } l = 1, \dots, L, \quad (12)$$

218 where the subscripts  $k$  and  $l$  are the indices of the ensemble member and the iteration, respectively; the superscripts  $u$   
219 and  $f$  are the updated and forecast parameters or states, respectively;  $N_e$  is the number of ensemble members;  $L$  is the  
220 number of iterations;  $m_{k,l}^f$  and  $m_{k,l}^u$  are the  $k$ th ensemble member of the forecast/prior and updated/posterior  
221 parameters, respectively, at the  $l$ th iteration;  $d_{obs}$  is the observation;  $z_k$  is the observation noise sampled from



222 independent standard normal distributions for the  $k$ th ensemble member;  $d_{k,l}^f$  is the  $k$ th ensemble member of the  
223 predicted observation states by the model using  $m_{k,l}^f$ ;  $C_{MD,l}^f$  is the cross-covariance matrix between the prior parameters  
224  $m_l^f$  and the predicted observation states  $d_l^f$ ;  $C_{DD,l}^f$  is the auto-covariance matrix of the predicted observation states  $d_l^f$ ;  
225  $C_D$  is the auto-covariance matrix of the observation error; and  $\alpha_l$  is the inflation coefficient at the  $l$ th iteration with the  
226 sum of all  $\alpha_l$  equal to one.

227 Here, the assimilation starts with taking the ensemble model parameters/states in Step 3 and the provided observations,  
228 and calculates the posterior parameters using ensemble Kalman filter, updates the prior parameters with the current  
229 posterior for the next iteration, and then repeats the whole process for multiple times (typically 3 to 5 iterations, as  
230 defined by the user). The final estimated parameters are obtained from the posterior parameter at the last iteration and  
231 are updated in the parameter HDF5 file. The parameter estimation is implemented in a way that allows assimilating  
232 either a single (e.g., Test Case 1) or multiple observed species simultaneously through a simple change of the inputs.  
233 For example, if temporal experimental or field data is available for oxygen, pH, and total carbon, all these data sources  
234 could be simultaneously fit to, with only minor adjustments to Jupyter notebook.

### 235 2.3.5 Step 5 – Simulation Output and Visualization

236 The last step performs the ensemble simulation of the biogeochemical modeling a final time using the estimated  
237 parameters in Step 4. Optionally, users can further pick the realization with the best performance. The user has the  
238 option to select their preferred goodness of fit metric from the following options as a means for selecting the best  
239 performing simulation: R-squared ( $R^2$ ), Root Mean Squared Error (RMSE), Modified Kling-Gupta Efficiency  
240 (MKGE), Nash-Sutcliffe Model Efficiency Coefficient (NSE), or Correlation Coefficient (CorC). Based on the  
241 selection, the final time series of aqueous chemistry, oxygen consumption,  $\text{CO}_2$  production, and lambda binned, and  
242 total organic carbon concentrations will be computed and plotted.

## 243 3 Test Cases

### 244 3.1 Test Case 1 - Oxygen Depletion Incubation Experiments.

245 In the first illustrative example, the lambda pipeline was used to fit three lambda model parameters ( $\mu_{max}$ ,  $V_h$ , and  $CC$ )  
246 to laboratory incubation experiments where oxygen levels were measured over two hours in a closed reactor. The  
247 incubation experiments were completed as part of the Worldwide Hydrobiogeochemistry Observation Network for  
248 Dynamic River Systems (WHONDRS) program (Goldman et al, 2020). For these incubations, sediment was taken  
249 from three locations within a stream (i.e., upstream, midstream, and downstream) in the Yakima River Basin in  
250 Washington, USA for subsequent laboratory respiration experiments. FTICR-MS was used to determine the OM  
251 chemistry from each sediment sample, resulting in variable formulae being identified in each sample. Formulae  
252 assignments for all the samples included herein were completed using formularity (Tolic et al., 2017). Total dissolved  
253 organic carbon concentration paired with the FTICR-MS sample and biomass measurements taken at the start of each  
254 experiment were used as the initial concentrations for each of the simulations. Due to the absence of quantitative data  
255 related to how the total carbon mass is distributed between various the OM compounds, the total carbon concentration



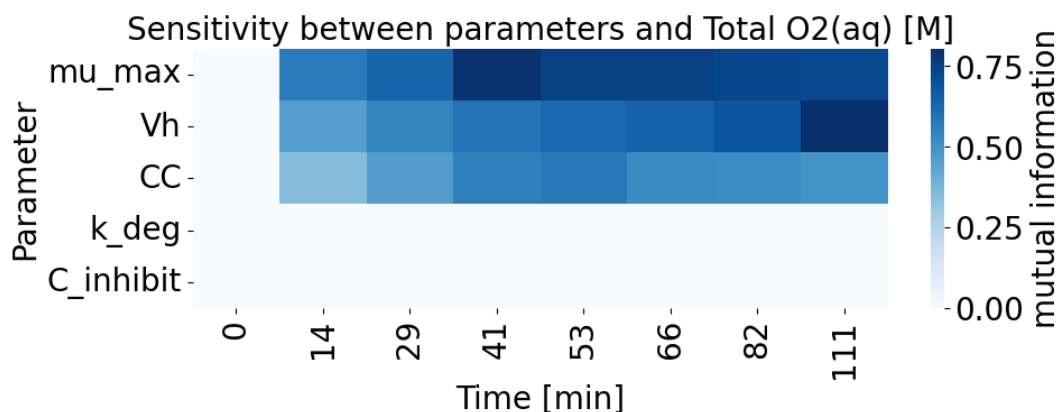
256 (on a per-C basis) was assumed to be split equally between each of the  $\lambda$  bins. The total organic carbon concentration  
257 was distributed into each  $\lambda$  bin using Eq. (13). While this assumption results in equal distribution of carbon between  
258 the bins, consequently, it assigns different initial species concentrations due to varying carbon concentrations between  
259 the molecules.

$$260 \quad [C_{\lambda bin}]_0 = \frac{[TOC]}{n_{\lambda bin} n_{C_{\lambda bin}}} \quad (13)$$

261 Where:  $[C_{\lambda bin}]_0$  is the initial species concentration in each  $\lambda$  bin [ $\text{mol} \cdot \text{L}^{-1}$ ];  $TOC$  is the total organic carbon measured  
262 [ $\text{mol-carbon} \cdot \text{L}^{-1}$ ];  $n_{\lambda bin}$  is the number of  $\lambda$  bins [-]; and  $n_{C_{\lambda bin}}$  is the number of carbon molecules in the assumed  
263 formula for the  $\lambda$  bins [ $\text{mol-carbon} \cdot \text{mol-molecule}^{-1}$ ].

264 Using the Lambda-PFLOTRAN workflow, the FTICR-MS data from each laboratory experiment was digested into  
265 the corresponding  $\lambda$  bins to create the individual reaction network. The Jupyter Notebook for this example is  
266 “Test\_Case1-WHONDRS.ipynb”. The resulting  $\lambda$  binning and associated reaction network for Test Case 1a are shown  
267 in Figure 2 and Table 1. Test cases 1b and 1c are in the Supporting Information (Fig. S1 - S2 and Tables S2 - S3). The  
268 calculated parameter sensitivity is shown in Figure 3, which indicates the results highly sensitive to all three  
269 parameters, in particular  $\mu_{max}$  and  $V_h$  more so than and  $CC$ .

270



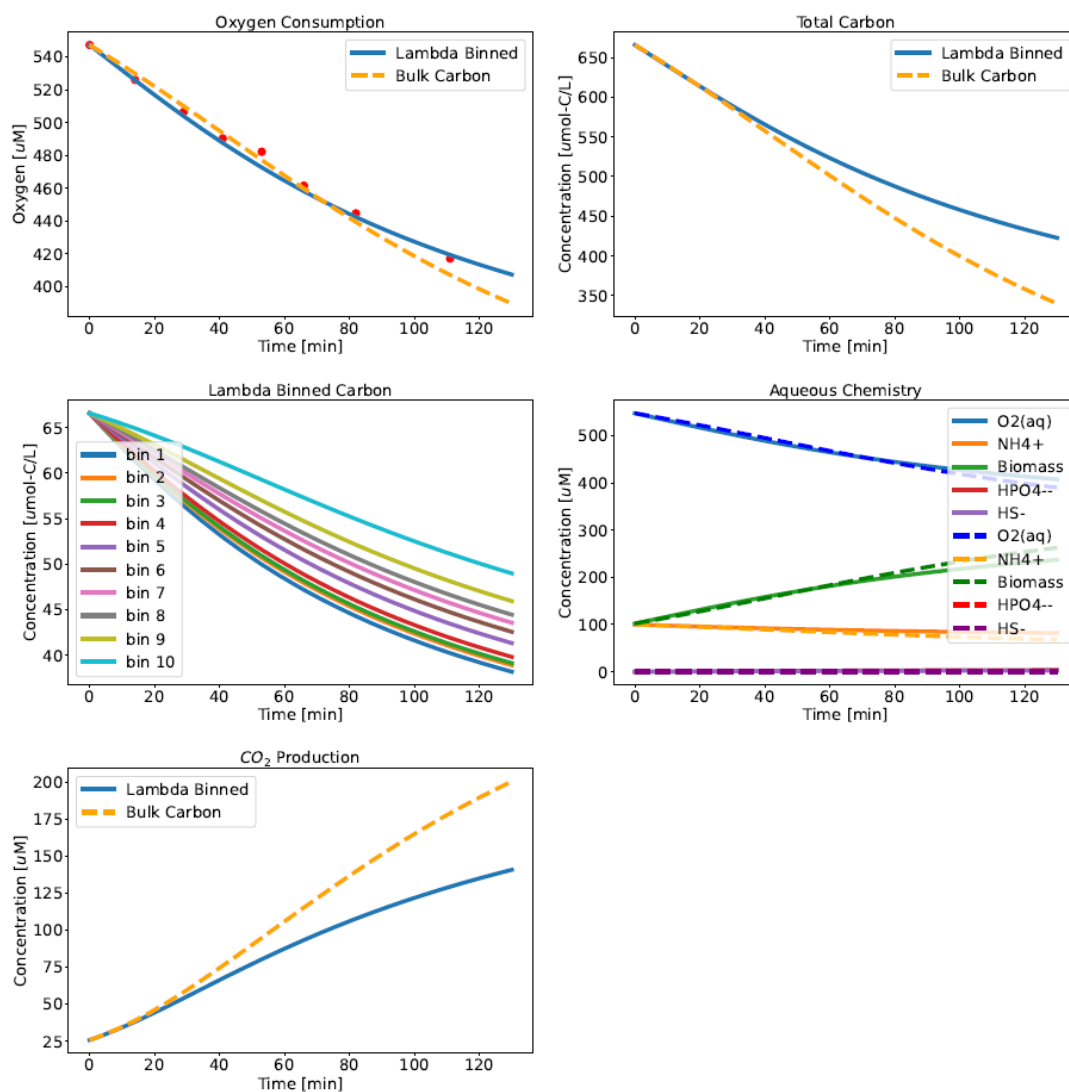
271

272 **Figure 3:** Illustrative Example of Sensitivity Analysis Output during Parameter Estimation. Example shown here provides the  
273 sensitivity of three fitted parameters ( $\mu_{max}$ ,  $V_h$ , and  $CC$ ) on temporal aqueous  $O_2$  concentrations as a function of time.

274 Lambda expression parameters were fit to the provided experimental oxygen data and the final fit to the experimental  
275 data and corresponding carbon consumption (individual and total) and aqueous chemistry is displayed in Figure 4 (and  
276 in the supporting information Fig. S2 and S3 for Test Cases 1b and c, respectively). The workflow was also run  
277 assuming a generic OM form of  $CH_2O$ , allowing comparison between using information for lambda binned OM  
278 obtained from FTICR-MS (Figure 4). In this case, the same set of lambda parameters were fit to the oxygen



279 consumption experimental data, which also resulted in successful fit ( $R^2 = 0.990$  for lambda binned model;  $R^2 = 0.987$   
280 for bulk model).



281  
282 **Figure 4:** Test Case 1a Results – Oxygen Consumption (top left) where Lambda-PFLOTTRAN workflow was used to fit (blue line)  
283 to experimental respiration data (red dots) and the corresponding Total Carbon Consumption (top right); Individual Organic Matter  
284 Consumption by  $\lambda$  bin (middle left); corresponding biogeochemistry including O<sub>2</sub> (aq) (blue); Biomass (green); NH<sub>4</sub><sup>+</sup> (orange);  
285 HS<sup>-</sup> (purple); and HPO<sub>4</sub><sup>2-</sup> (red) (middle left); and CO<sub>2</sub> production (bottom left) for the upstream incubation. The dashed orange  
286 lines in the top two figures show simulation results assuming a generic OM species of CH<sub>2</sub>O for comparison. Fitted values for the  
287 lambda binned model are  $\mu_{\max} = 0.25 \text{ min}^{-1}$ ,  $V_h = 9.7 \text{ m}^3$ , and  $CC = 0.49 \text{ M}$  ( $R^2 = 0.990$ ), and fitted bulk OM CH<sub>2</sub>O model value  
288 are  $\mu_{\max} = 0.05 \text{ min}^{-1}$ ,  $V_h = 3.3 \text{ m}^3$ , and  $CC = 0.58 \text{ M}$  ( $R^2 = 0.987$ ).

289

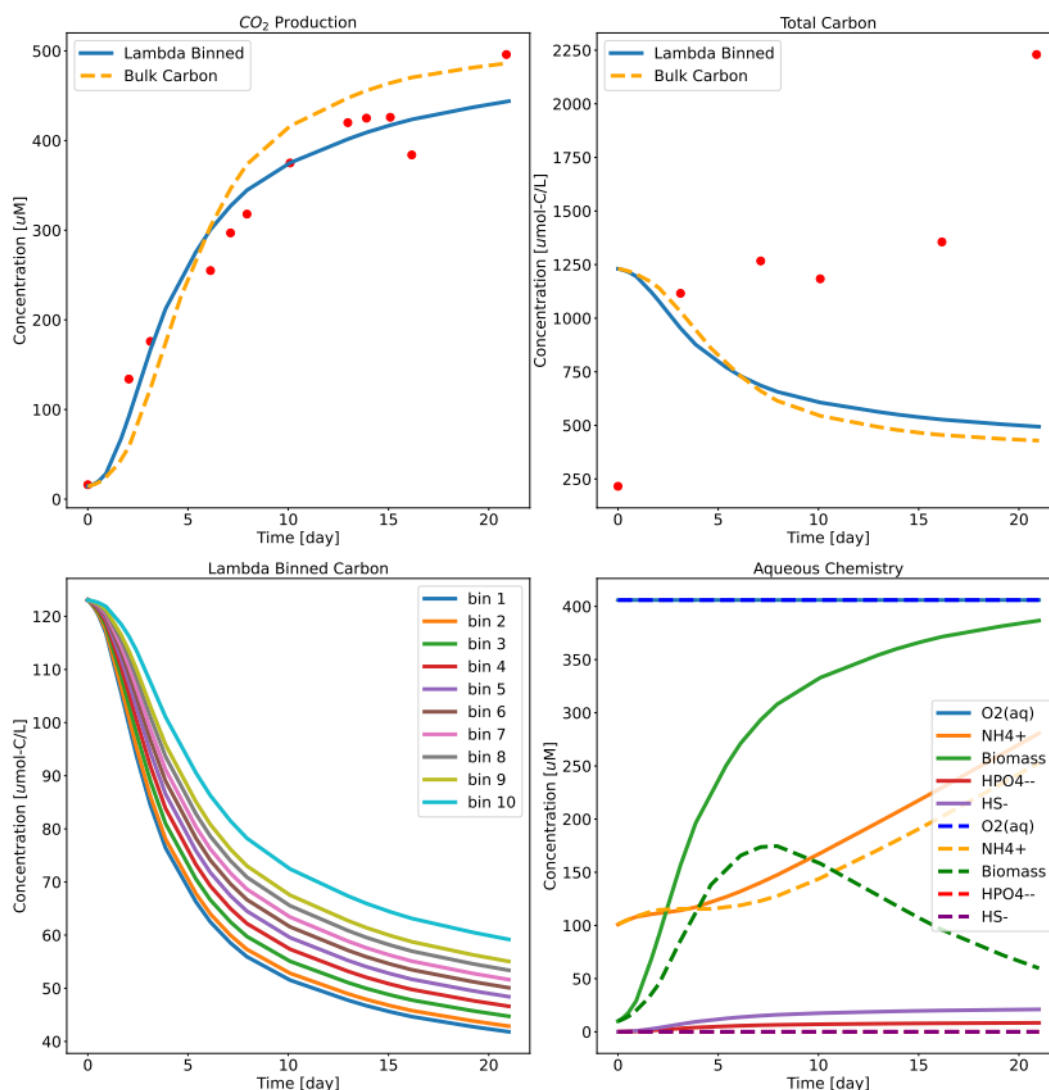


290 However, even over the short time frame of this simulation, the difference between assuming the generic  $\text{CH}_2\text{O}$  and  
291 using the more detailed organic matter chemistry resulted in different predictions of total carbon and  $\text{CO}_2$  generation.  
292 The bulk OM model predicts more carbon consumption and greater  $\text{CO}_2$  production than the binned lambda model.  
293 The bulk OM model estimates that 65% of the initial total carbon is consumed over the first 120 mins, whereas the  
294 lambda binned model predicts 54% consumption. Similarly, the bulk OM model estimates approximately 41% more  
295  $\text{CO}_2$  generation as compared the lambda binned model. The effects on aqueous chemistry over this short duration are  
296 more muted, albeit still present.

### 297 **3.2 Test Case 2 - Respiration Incubation Experiments.**

298 Test Case 2 uses soil respiration incubation data from Ward et al. (2023) aimed at investigating the influence of soil  
299 type, oxygen condition (aerobic vs. anaerobic), and seawater exposure (fresh vs. saline) on respiration extent and rate.  
300 For these experiments, temporal measurements were collected for  $\text{CO}_2$  generation, dissolved organic carbon (DOC),  
301 organic matter formulas via FTICR-MS and other bulk aqueous chemistry (i.e., pH,  $\text{NH}_4^+$ , and other metals and ions)  
302 creating a rich dataset for calibration of system specific lambda model parameters. These incubations were setup by  
303 adding dry soil to the reactor and then adding water (resulting in a soil:water ratio ranging from 1:11 to 1:16). The soil  
304 and water were shaken vigorously for five minutes, and then sampled for the initial time point prior to officially  
305 starting the incubation. For the aerobic experiments, the reactor headspace was cycled every 24 hours to measure  $\text{CO}_2$   
306 generated but also to ensure the system was kept aerobic; this was only performed five days per week, with no  
307 measurements taken on the weekend due to logistical constraints. Upon experiment completion, the increase in DOC  
308 concentrations indicated organic carbon was being kinetically released from the soil into the aqueous phase over the  
309 course of the 21-day experiment. Similarly, measured  $\text{NH}_4^+$  concentrations also increased during the experiment. To  
310 address this, a source of nitrogen was assumed to be released from the soil as well ( $N_{\text{release}}$ ). Both carbon and nitrogen  
311 release are included in this example and are assumed to follow a zero-order constant release rate. Any organic carbon  
312 released from the soil was fractionated into each  $\lambda$  bin on the same per-carbon basis assumed for the initial total organic  
313 carbon. This was implemented through a dependent function that calculated the release of carbon into each  $\lambda$  bin based  
314 on a fitted single bulk  $k_{\text{release}}$  rate. Mathematically in PFLOTRAN the constant oxygen conditions were implemented  
315 through a gas-liquid partitioning expression with a fast exchange term.

316 The workflow was used to fit  $\mu_{\text{max}}$ ,  $V_{\text{h}}$ ,  $CC$ ,  $k_{\text{deg}}$ , as well as  $k_{\text{release}}$ , to the temporal  $\text{CO}_2$  generation for a single aerobic  
317 soil incubation (Figure 5). The Jupyter Notebook for this example is “Test\_Case2-Colloids.ipynb”.



318

319

320

321

322

323

324

325

326

327

328

**Figure 5.** Test Case 2 Results – CO<sub>2</sub> production (top left) where Lambda-PFLOTRAN workflow was used to fit (blue line) to experimental respiration data (red dots) and the corresponding Total Organic Carbon (top right); Individual Organic Matter Consumption by  $\lambda$  bin (bottom left) and corresponding biogeochemistry including O<sub>2</sub> (aq) (blue); Biomass (green); NH<sub>4</sub><sup>+</sup> (orange); HS<sup>-</sup> (purple); and HPO<sub>4</sub><sup>-</sup> (red) (bottom right). Dots indicate experimental data. The dashed orange lines in the top two figures show simulation results assuming a generic OM species of CH<sub>2</sub>O for comparison. Fitted parameters for lambda binned model were  $k_{\text{release}} = 5.5 \times 10^{-12} \text{ day}^{-1}$ ;  $\mu_{\text{max}} = 37.6 \text{ day}^{-1}$ ,  $V_h = 5.0 \text{ m}^3$ ,  $CC = 0.12 \text{ M}$ , and  $k_{\text{deg}} = 1 \times 10^{-3} \text{ day}^{-1}$  ( $R^2 = 0.953$ ) and fitted bulk OM CH<sub>2</sub>O model values were  $k_{\text{release}} = 2.0 \times 10^{-12} \text{ day}^{-1}$ ;  $\mu_{\text{max}} = 47 \text{ day}^{-1}$ ,  $V_h = 1.0 \text{ m}^3$ ,  $CC = 0.77 \text{ M}$ , and  $k_{\text{deg}} = 0.15 \text{ day}^{-1}$  ( $R^2 = 0.909$ ).

The best fit results indicate a superior fit using the lambda binned OM over the bulk OM model and in fact, the bulk model is unable to successfully capture the temporal evolution of the CO<sub>2</sub>. It should be noted that both model fits are highly sensitive to the allowable parameter space as user defined by the lower and upper parameter bounds. For the



329 purposes for showcasing the workflow, five parameters were estimated in this test case example, and as a result the  
330 models are likely over parametrized given the amount of data available. Any additional experimental data, either  
331 collected during incubations or through independent experiments (e.g., carbon release from the soil in an abiotic  
332 system), would be expected to help constraint the model and improve parameterization.

#### 333 **4 Conclusions**

334 Overall, Lambda-PFLOTRAN workflow provides an important linkage between molecular scale organic matter  
335 characterization and reactive transport simulations. This workflow allows for the influence of organic matter  
336 composition to be utilized within simulators to provide a more comprehensive understanding of the system chemistry  
337 and behavior, moving beyond the standard assumption of bulk organic matter chemistry and composition. While there  
338 are current limitations due to how composition is characterized and quantified, this workflow connecting  
339 characterization information to simulations is an important advancement that can be refined as these laboratory  
340 techniques improve over time.

341 One of the major limitations surrounding this method, is the lack of understanding of organic matter compound  
342 bioavailability, resulting in a large conceptual gap as to how various organic carbon compounds may be utilized by  
343 microbes. In the absence of such information, all identified organic matter molecules are assumed to have equal  
344 bioavailability within this modeling framework when, in reality, compounds will exhibit varying degrees of  
345 bioavailability depending on factors such as associated size fraction, carbon pool, and environmental factors (Schmidt  
346 et al., 2011; Ahamed et al., 2023). Until improved understanding is established to discern individual compound  
347 bioavailability, this will remain as a limitation.

348 Another limitation of this method resides around the analytical limitations of organic carbon characterization and  
349 quantification. For instance, FTICR-MS focuses on water soluble organic matter which may provide a bias in the  
350 types of carbon identified by this technique (Tfaily et al., 2017). Additionally, as mentioned previously, FTICR-MS  
351 is qualitative, it does not provide structural information and will not differentiate between different isomers that have  
352 the same molecular formulas, it is only able to identify molecular formula is present or absent and not the concentration  
353 associated with each peak. Here, this has been addressed by assuming equal distribution of total carbon between the  
354 formulas within each  $\lambda$  bin on a per-carbon basis. This caveat can be easily updated in the workflow if new analytical  
355 advances are made that provide more quantitative information. Some existing approaches could be suitable for this  
356 type of modeling such as using quantitative biomarkers that cover major compound classes (Kim and Blair, 2023);  
357 but further advances in obtaining both high resolution and quantitative OM characterization would greatly aid in how  
358 we understand and model ecosystems.

359



360 **Acknowledgements:**

361 This research was performed under a variety of interdisciplinary projects including the U.S. Department of Energy  
362 (DOE) sponsored Office of Science, Office of Biological and Environmental Research (BER), Environmental System  
363 Science (ESS) Program, IDEAS-Watersheds, River Corridor Scientific Focus Area (SFA), the Environmental  
364 Molecular Sciences Laboratory User Facility sponsored by the Biological and Environmental Research program under  
365 Contract No. DE-AC05-76RL01830, and COMPASS-FME, a multi-institutional project supported by DOE-BER as  
366 part of the Environmental System Science Program. This study used data from the Worldwide Hydrobiogeochemistry  
367 Observation Network for Dynamic River Systems (WHONDRS). This paper describes objective technical results and  
368 analysis. The work was performed at the Pacific Northwest National Laboratory (PNNL). Any subjective views or  
369 opinions that might be expressed in the paper do not necessarily represent the views of the U.S. Department of Energy  
370 or the United States Government.

371

372 **Code Availability:**

373 The source code, installation requirements, example test case notebooks, and associated data are available in ESS  
374 DIVE at <https://doi.org/10.15485/2281403>

375

376 **Author Contribution:**

377 KM: conceptualization, formal analysis, methodology, software, writing- original draft preparation; PJ: methodology,  
378 software, writing- original draft preparation; GH: methodology, software, writing-review & editing; TA: data curation,  
379 software, writing-review & editing; HS: methodology, writing-review & editing; RK: supervision; NW: supervision,  
380 writing-review & editing; MB: investigation; RC: investigation; QZ: investigation; VG: investigation, data curation;  
381 AR: investigation; XC: conceptualization, investigation, writing-review & editing

382

383 **Competing Interests:** The authors declare that they have no conflict of interest.

384 **References**

- 385 Bahureksa, W., Tfaily, M. M., Boiteau, R. M., Young, R. B., Logan, M. N., McKenna, A. M., & Borch, T. (2021).  
386 Soil organic matter characterization by Fourier transform ion cyclotron resonance mass spectrometry (FTICR MS): A  
387 critical review of sample preparation, analysis, and data interpretation. *Environmental science & technology*, 55(14),  
388 9637-9656, <https://doi.org/10.1021/acs.est.1c01135>
- 389 Cover, T. M., and Thomas, J. A. (2006). Elements of information theory (Wiley series in telecommunications and  
390 signal processing). Wiley-Interscience.
- 391 Emerick, A.A., Reynolds, A.C. (2013). Ensemble smoother with multiple data assimilation. *Comput. Geosci.* 55, 3–  
392 15. <https://doi.org/10.1016/j.cageo.2012.03.011>.
- 393 Faticchi, S., Manzoni, S., Or, D., & Paschalis, A. (2019). A mechanistic model of microbially mediated soil  
394 biogeochemical processes: a reality check. *Global Biogeochemical Cycles*, 33(6), 620-648.  
395 <https://doi.org/10.1029/2018GB006077>





- 396 Garayburu-Caruso, V., Stegen, J., Song, H.-S., Renteria, L., Wells, J., Garcia, W., et al. (2020). Carbon limitation  
397 leads to thermodynamic regulation of aerobic metabolism. *Environ. Sci. Technol. Lett.* 7, 517–524.  
398 <https://doi.org/10.1021/acs.estlett.0c00258>
- 399 Goldman A E ; Arnon S ; Bar-Zeev E ; Chu R K ; Danczak R E ; Daly R A ; Delgado D ; Fansler S ; Forbes B ;  
400 Garayburu-Caruso V A ; Graham E B ; Laan M ; McCall M L ; McKeever S ; Patel K F ; Ren H ; Renteria L ; Resch  
401 C T ; Rod K A ; Tfaily M ; Tolic N ; Torgeson J M ; Toyoda J G ; Wells J ; Wrighton K C ; Stegen J C ; WHONDRS  
402 Consortium T (2020): WHONDRS Summer 2019 Sampling Campaign: Global River Corridor Sediment FTICR-MS,  
403 Dissolved Organic Carbon, Aerobic Respiration, Elemental Composition, Grain Size, Total Nitrogen and Organic  
404 Carbon Content, Bacterial Abundance, and Stable Isotopes (v8). River Corridor and Watershed Biogeochemistry SFA,  
405 ESS-DIVE repository. Dataset. doi:10.15485/1729719 accessed via [https://data.ess-  
406 dive.lbl.gov/datasets/doi:10.15485/1729719](https://data.ess-<br/>406 dive.lbl.gov/datasets/doi:10.15485/1729719) on 2023-12-28
- 407 Hammond, G. E., Lichtner, P. C., & Mills, R. T. (2014). Evaluating the performance of parallel subsurface simulators:  
408 An illustrative example with PFLOTTRAN. *Water resources research*, 50(1), 208–228.  
409 <https://doi.org/10.1002/2012WR013483>
- 410 Hammond, G.E. (2022) The PFLOTTRAN Reaction Sandbox, *Geoscientific Model Development*, 15, 1659–1676,  
411 <https://doi.org/10.5194/gmd-15-1659-2022>.
- 412 Jiang P., Chen, X., Chen, K., Anderson, J., Collins, N., Gharamti, M. (2021) DART-PFLOTTRAN: An ensemble-based  
413 data assimilation system for estimating subsurface flow and transport model parameters. *Environmental Modelling &  
414 Software*, Volume 142, <https://doi.org/10.1016/j.envsoft.2021.105074>.
- 415 Jiang, P., Son, K., Mudunuru, M.K. and Chen, X. (2022). Using mutual information for global sensitivity analysis on  
416 watershed modeling. *Water Resources Research*, 58(10), <https://doi.org/10.1029/2022WR032932>
- 417 Kim, J., Blair, N.E. Biomarker heatmaps: visualization of complex biomarker data to detect storm-induced source  
418 changes in fluvial particulate organic carbon. *Earth Sci Inform* 16, 2915–2924 (2023). [https://doi.org/10.1007/s12145-  
419 023-01039-y](https://doi.org/10.1007/s12145-<br/>419 023-01039-y)
- 420 Kinzelbach, W., Schafer, W., and Herzer, J. (1991). Numerical modeling of natural and enhanced  
421 denitrification processes in aquifers. *Water Resources Research*, 27(6):1123–1135.  
422 <https://doi.org/10.1029/91WR00474>
- 423 Kleerebezem, R., & Van Loosdrecht, M. C. (2010). A generalized method for thermodynamic state analysis of  
424 environmental systems. *Critical Reviews in Environmental Science and Technology*, 40(1), 1–54.  
425 <https://doi.org/10.1080/10643380802000974>
- 426 Kluyver, T., Ragan-Kelley, B., Pérez, F., Granger, B. E., Bussonnier, M., Frederic, J., ... & Willing, C. (2016). Jupyter  
427 Notebooks—a publishing format for reproducible computational workflows. *Elpub*, 87–90. 10.3233/978-1-61499-649-  
428 1-87
- 429 Lehmann, J., Hansel, C.M., Kaiser, C. *et al.* (2020). Persistence of soil organic carbon caused by functional  
430 complexity. *Nat. Geosci.* 13, 529–534 <https://doi.org/10.1038/s41561-020-0612-3198718>



- 431 Robertson, A. D., Paustian, K., Ogle, S., Wallenstein, M. D., Lugato, E., & Cotrufo, M. F. (2019). Unifying soil  
432 organic matter formation and persistence frameworks: the MEMS model. *Biogeosciences*, 16(6), 1225-1248.  
433 <https://doi.org/10.5194/bg-16-1225-2019>
- 434 Schmidt, M., Torn, M., Abiven, S. et al. (2011) Persistence of soil organic matter as an ecosystem  
435 property. *Nature* 478, 49–56. <https://doi.org/10.1038/nature10386>
- 436 Stegen, J. C., Garayburu-Caruso, V. A., Danczak, R. E., Goldman, A. E., Renteria, L., Torgeson, J. M., and Wells, J.  
437 R.: Hyporheic Zone Respiration is Jointly Constrained by Organic Carbon Concentration and Molecular Richness,  
438 EGU sphere [preprint], <https://doi.org/10.5194/egusphere-2022-613>, 2023.
- 439 Song, H.S., Stegen, J.C., Graham, E.B., Lee, J.Y., Garayburu-Caruso, V.A., Nelson, W.C., Chen, X., Moulton, J.D.  
440 and Scheibe, T.D. (2020). Representing organic matter thermodynamics in biogeochemical reactions via substrate-  
441 explicit modeling. *Frontiers in microbiology*, 11, p.531756. <https://doi.org/10.3389/fmicb.2020.531756>
- 442 Stegen, J.C., Johnson, T., Fredrickson, J.K. et al. (2018). Influences of organic carbon speciation on hyporheic  
443 corridor biogeochemistry and microbial ecology. *Nat Commun* 9, 585 <https://doi.org/10.1038/s41467-018-02922-9>
- 444 Stephanopoulos, George, Aristos A. Aristidou, and Jens Nielsen. (1998) Metabolic engineering: principles and  
445 methodologies.
- 446 Tfaily, M. M., Chu, R. K., Toyoda, J., Tolić, N., Robinson, E. W., Paša-Tolić, L., & Hess, N. J. (2017). Sequential  
447 extraction protocol for organic matter from soils and sediments using high resolution mass spectrometry. *Analytica*  
448 *chimica acta*, 972, 54-61.
- 449 Tolic, N., Liu, Y., Liyu, A., Shen, Y., Tfaily, M. M., Kujawinski, E. B., ... & Hess, N. J. (2017). Formularity: software  
450 for automated formula assignment of natural and other organic matter from ultrahigh-resolution mass spectra.  
451 *Analytical chemistry*, 89(23), 12659-12665.
- 452 Wang, G., W.M. Post and M.A. Mayes (2013). Development of microbial-enzyme-mediated decomposition model  
453 parameters through steady-state and dynamics analyses, *Ecological Applications*, 23(1), 255-272,  
454 <https://doi.org/10.1890/12-0681.1>
- 455 Ward, N.D., Keil, R.G., Medeiros, P.M., Brito, D.C., Cunha, A.C., Dittmar, T., Yager, P.L., Krusche, A.V., Richey,  
456 J.E. (2013) Degradation of terrestrially derived macromolecules in the Amazon River. *Nature Geoscience*. 6 (7), 530-  
457 533. <https://doi.org/10.1038/ngeo1817>
- 458 Ward, N.D, Muller, K.A., Chen, X., Zhao, Q., Chu, R., Cheng, Z., Wietsma, T.W., Kukkadapu, R.K. (2023).  
459 Interactive Effects of Salinity, Redox State, Soil type, and Colloidal Size Fractionation on Greenhouse Gas Production  
460 in Coastal Wetland Soils. ESS Open Archive. <https://doi.org/10.31223/X5FM0N>